Multiple Scenarios of Low-Temperature Nucleation in Simple Liquids

Mengyuan Zhan,[1] Yanshuang Chen,[2] Zhehua Jiang,[1] Ning Xu,[1,*] and Peng Tan[2,†]
[1]Hefei National Research Center for Physical Sciences at the Microscale, CAS Key Laboratory of Microscale Magnetic Resonance and Department of Physics, University of Science and Technology of China, Hefei 230026, People's Republic of China
[2]State Key Laboratory of Surface Physics and Department of Physics, Fudan University, Shanghai 200433, People's Republic of China

(Received 16 September 2022; accepted 4 April 2023; published 25 April 2023)

Usually, sufficient supercooling of a liquid is employed to bypass the free energy barrier and speed up crystallization. However, lowering the temperature T induces new issues competing with the crystallization, e.g., slow particle motion, geometric frustration, and the glass formation, which complicates our understanding of crystal growth. Here we systematically study the low-temperature nucleation kinetics discriminated by the maximum nucleation rate temperature T_d and the glass transition temperature T_g. At T_d, the ratio of the precursor and geometrically frustrated particles reaches the maximum. When $T_g < T < T_d$, nucleation kinetics is characterized by the subdiffusive slow particle motion, the high degrees of geometric frustration, and the saturation of precursors. In this regime, nucleation can proceed through the diffusionless-like ordering of precursors. Near T_g, there is a crossover regime, where geometrically frustrated particles percolate and the glass formation strongly slows down the nucleation. When $T < T_g$, diffusionless nucleation is obstructed due to the weak vibrational motion and the mechanical stability of the glassy state.

DOI: 10.1103/PhysRevLett.130.178201

Liquid melts upon rapid and deep quenching could either crystallize or vitrificate [1–5]. Exploring the crystallization kinetics at the low-temperature regime is of fundamental importance to condensed matter physics and material sciences [6,7]. In many industrial applications, rapid and deep quenching is often used, but it is crucial to prevent the vitrification, increase the speed of crystallization, and control the quality and morphology of crystals to be formed. However, compared with the clear understanding of crystallization under slow and shallow quenching (high-temperature regime) [1–3,8–14], the crystallization kinetics at the low-temperature regime still remains elusive [15–19].

The nucleation time, τ_N, and the α structural relaxation time of a liquid, τ_α, are two characteristic timescales describing the crystallization kinetics. In the high-temperature regime, i.e., above the kinetic spinodal temperature T_{sp} that the nucleation barrier is comparable to k_BT with k_B and T being the Boltzmann constant and temperature, the liquid melt is metastable and the long-time diffusive dynamics dominates the nucleation process [20]. As a result, $\tau_N \gg \tau_\alpha$. For this case, previous studies revealed the spontaneous fluctuation of liquid regions with relatively high bond orientational order prior to the formation of critical nucleus [11,12,21]. Additionally, the icosahedronlike motifs start to participate in the nucleation process and contribute to the formation of amorphous precursors of crystal nuclei close to T_{sp} [22–26]. It has been long believed that icosahedrons frustrate crystallization and the slow-diffusion hinders crystallization. We may thus expect the drastic slowing down of crystallization below T_{sp} upon rapid and deep quenching. However, many studies find that the fastest crystallization happens at the temperature much lower than T_{sp}. In this case, τ_N should be smaller than τ_α, but a clear understanding of how the fastest crystallization operates is still lacking.

Another puzzle is how fast crystallization ceases upon vitrification at low temperatures, i.e., close to the experimental glass transition temperature T_g. In this regime, the geometric frustration fights against the crystallization [16–18,27,28], and the particles diffuse slowly, presumably in the subdiffusive way as good glass formers do [4,5]. Previous studies have revealed that both precursorlike and icosahedronlike structures grow up in rapid-quenching liquid towards the glass transition [19]. These phenomena imply that precursor structures, geometric frustration, and short-time diffusion may interplay to affect the crystallization and vitrification close to T_g. Under such conditions, it is straightforward to suspect that the fast-crystallization mode operates via small particle movements, while the vitrification tends to "freeze" such ordering. This competition may push the glass transition to ultralow temperatures, below which the growth of the local ordering is highly suppressed and the dynamics of glass samples is dominated by small-magnitude vibrational motion. However, this scenario is still under speculation and requires elucidation.

Here we study the low-temperature nucleation kinetics using model systems consisting of monodisperse spherical particles. Besides the glass transition temperature T_g, we

find another crossover temperature T_d where both the nucleation rate I and the ratio of the precursor and geometrically frustrated particles show a maximum. When $T_g < T < T_d$, the nucleation proceeds through the diffusionlesslike ordering of nucleation precursors. The specific characteristics in this temperature regime include the subdiffusive slow particle motion, the high degrees of geometric frustration, and the saturation of precursors. Interestingly, there is a crossover temperature regime right above T_g, where the geometrically frustrated particles percolate and the diffusionlesslike ordering quickly decays and ceases at T_g, indicating that the glass formation has started to strongly compete with the nucleation. However, in this crossover, the thermal energy is not yet low enough to stop the sluggish further ordering of precursors on the backbone of geometrically frustrated particles. This competition indeed pushes T_g to ultralow temperatures, which is about $T_d/10$, as speculated. When $T < T_g$, the percolation of geometrically frustrated particles and weak vibrational motion prevail over the further ordering of precursors. As a result, the system is mechanically stable and the diffusionless crystallization is obstructed.

Our systems contain N spherical particles with diameter σ and mass m simulated using periodic boundary conditions within a three-dimensional cubic cell with side length L. The particles interact via the pairwise potential

$$U(r_{ij}) = \epsilon S(r_{ij})\Theta\left(1 - \frac{r_{ij}}{r_c}\right), \tag{1}$$

where r_{ij} is the interparticle distance, ϵ is the characteristic energy scale of the interaction, $\Theta(x)$ is the Heaviside step function, r_c is the cutoff of the potential, and $S(r_{ij})$ represents the functional form of the interaction. To generalize our results, we consider three distinct types of particle interactions, including Lennard-Jones (LJ), Hertzian (HZ), and Yukawa (YK), with

$$S(r_{ij}) = \left[\left(\frac{\sigma}{r_{ij}}\right)^{12} - \left(\frac{\sigma}{r_{ij}}\right)^{6}\right], \tag{2}$$

$$S(r_{ij}) = \left(1 - \frac{r_{ij}}{\sigma}\right)^{5/2}, \tag{3}$$

$$S(r_{ij}) = \frac{\sigma}{r_{ij}}\exp\left(-\kappa\frac{r_{ij}}{\sigma}\right), \tag{4}$$

respectively, where κ/σ is the inverse Debye screening length. We set the cutoff length, r_c, to be 2.5σ, σ, and 10σ for LJ, HZ, and YK potentials, respectively. The units of mass, energy, and length are set to be m, ϵ, and σ. The time is thus in units of $\sqrt{m\sigma^2/\epsilon}$. The temperature T is in units of ϵ/k_B. The dimensionless number densities $\rho = N\sigma^3/L^3$ are 1.2, 1.8, and 0.036 for LJ, HZ, and YK potentials, respectively. For the YK potential, we set $\kappa/\sigma = 1$. Here we show results of $N = 32\,000$ particles and have checked that our findings do not show strong system size dependence.

We first equilibrate liquid states at $T > T_m$ and then rapidly quench them to the target temperature below T_m. Here T_m is the effective melting temperature defined in the Supplemental Material (SM) [29]. At all temperatures, we perform molecular dynamics simulations with the canonical ensemble, and the results are averaged over 50 independent runs. Upon rapid quenching, particles form various local structures evolving with time and competing with each other [37–39]. We use the Steinhardt bond orientational order parameters based on the spherical harmonics [21,30,40–45] to identify the local structural orders. See the SM [29] for the definitions.

For all three systems studied here, the face-centered-cubic (FCC) or hexagonal-close-packed (HCP) structures are the stable ones. Perfect FCC and HCP structures have the maximum bond orientational order $q_6 = 0.57$ and $q_6 = 0.48$, respectively. We thus treat particles with $q_6 > 0.4$ as crystalline particles [11,24] and show in Fig. 1(a) the time evolution of the fraction of crystalline particles, $\phi_c(t)$,

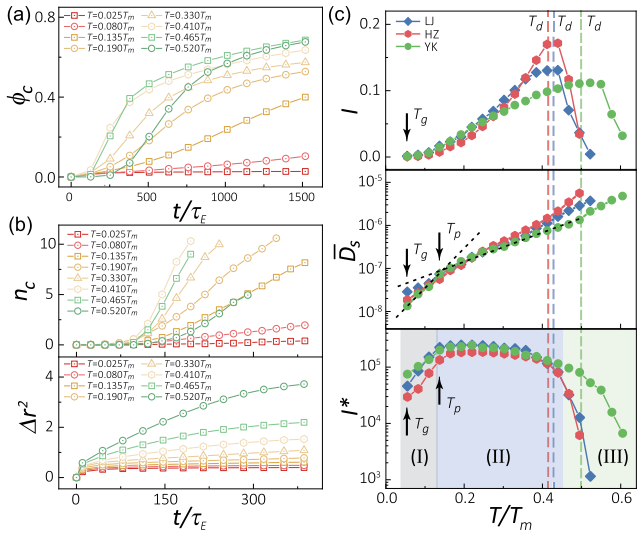

FIG. 1. Temperature dependence of early-stage crystallization. (a) Time evolution of the fraction of crystalline particles ϕ_c for the LJ system. (b) Time evolution of the number of crystal nuclei, n_c (top panel) and mean square displacement Δr^2 (bottom panel) for the LJ system. The time t in (a) and (b) is scaled by the Einstein frequency τ_E^{-1}. (c) T dependence of the crystal growth rate I (top panel), short-time diffusion constant $\bar{D}_s$ (middle panel), and the reduced crystal growth rate I^* (bottom panel) for the LJ, HZ, and YK systems. The arrows specify the approximate locations of the characteristic temperatures T_p for the three systems and T_g for LJ and YK (T_g for HZ is a little higher and not shown). The vertical dashed lines specify T_d for the three systems. The black dotted lines in the middle panel indicate distinct behaviors across T_p. We distinguish different temperature regimes with different colors in the bottom panel.

taking the LJ systems as the example. We scale the time t by the Einstein frequency τ_E^{-1}. Here $\tau_E = \sqrt{m/k}$, where $k = 3k_BT/\Delta r_p^2$ with $T = 0.5T_m$ and Δr_p^2 being the plateau value of the mean square displacement [46].

As expected, $\phi_c(t)$ in Fig. 1(a) shows nonmonotonic temperature dependence at low temperatures. Below the glass transition temperature T_g, which is about $0.04T_m$ for LJ and YK and $0.08T_m$ for HZ, $\phi_c(t)$ grows extremely slowly due to the obstruction of the glass formation (see Fig. S3 of the SM [29] for the definition of T_g). When $T > T_g$, the slow crystallization process begins to speed up until it reaches a crossover temperature T_d that the initial growth rate of $\phi_c(t)$ reaches the maximum. Above T_d, the initial growth of $\phi_c(t)$ slows down instead.

During the initial growth of $\phi_c(t)$, crystalline particles cluster into crystal nuclei that further grow up. Interestingly, we find the fastest nucleation around T_d, as seen from the time evolution of the nuclei number $n_c(t)$ in the top panel of Fig. 1(b) (nuclei consisting of over 80 crystalline particles are counted). We then estimate the nucleation rate I from the linear relation, $n_c(t) \approx I(t - t_0)$ after an onset time t_0 [11,47]. For all systems, $I(T)$ shows a maximum around T_d, as illustrated in the top panel of Fig. 1(c). T_d is about $0.4T_m$ for LJ and HZ and $0.5T_m$ for YK. This similar behavior of $I(T)$ implies unified structural or dynamical changes across T_d. Note that this Letter focuses on the early-stage crystallization right after the quenching. If we wait for a long time until crystallization finalizes, $n_c(t)$ will reach a maximum and decay afterwards to the order of one. Compared with the later stage, which involves the simpler growth and coalescence of nuclei, the early-stage crystallization concerned here is more interesting, complicated, and important to understanding the mechanisms of nucleation.

Let us first look into the dynamics of the deep-cooling liquid at the nucleation stage. The crystallizing liquid is highly in nonequilibrium at low temperatures. We thus examine the mean square displacement, $\Delta r^2(t) = \langle (1/N) \sum_{i=1}^{N} [\vec{r}_i(t) - \vec{r}_i(0)]^2 \rangle$, calculated within a time window comparable to the linear regime of $n_c(t)$ [see top panel of Fig. 1(b)]. Here, $\vec{r}_i(t)$ is the location of particle i at time t, and $\langle \cdots \rangle$ denotes the average over independent simulation runs. In Fig. 1(b) (bottom panel), we can see a subdiffusive character of $\Delta r^2(t)$ when $T < T_d$, which indicates the absence of the long-time liquid diffusion, i.e., many times of α structural relaxation, within the time window of low-temperature nucleation. We then select a time-dependent short-time diffusion constant, $D_s(t) = (1/6L^2)[d\Delta r^2(t)/dt]$, to characterize the motion, and plot the average value $\bar{D}_s$ over the time window within which $n_c(t)$ remains roughly linear in the middle panel of Fig. 1(c) (refer to Table SI of the SM [29] about the time windows to take the average).

We can clearly see a three-stage evolution of $\bar{D}_s(T)$ from high T to low T, separated by T_d and another crossover temperature T_p about $0.13 \sim 0.16T_m$ depending on systems. This three-stage character suggests that the nucleation kinetics below and above T_d is governed by subdiffusive and diffusive motion, respectively, and the glass formation on approaching T_g has an additional effect on reducing the subdiffusion when $T < T_p$.

The reduced crystal growth rate, $I^* = I/\bar{D}_s$, also displays a similar three-stage feature (from low T to high T): (I) a regime below T_p where I^* drops quickly on approaching T_g, (II) a T-insensitive regime between T_p and T_d where $I^*(T)$ is plateaulike, and (III) a regime above T_d where I^* drops again, as shown in bottom panel of Fig. 1(c). This three-stage character implies that the reduction of $\bar{D}_s$ below T_d is responsible for the drop of I.

Note that the short-time diffusion constant $\bar{D}_s$ defined here takes effect only in the rather nonequilibrium early stage of the crystallization, which should not be confused with the long-time diffusion constant calculated from the equilibrium diffusive behavior, $\Delta r^2 \sim t$. Therefore, a nonzero $\bar{D}_s$ does not mean that particles can indeed diffuse at long times. We thus plot in Fig. 2(a) the temperature evolution of the mean particle displacement, $\Delta r = \langle (1/N) \sum_{i=1}^{N} |\Delta \vec{r}_i| \rangle$, over the crystallization process from $\phi_c \approx 1\%$ to 30%, with $\Delta \vec{r}_i$ being the displacement of particle i and $\langle \cdots \rangle$ denoting the average over simulation runs. At low temperatures, Δr remains smaller than the

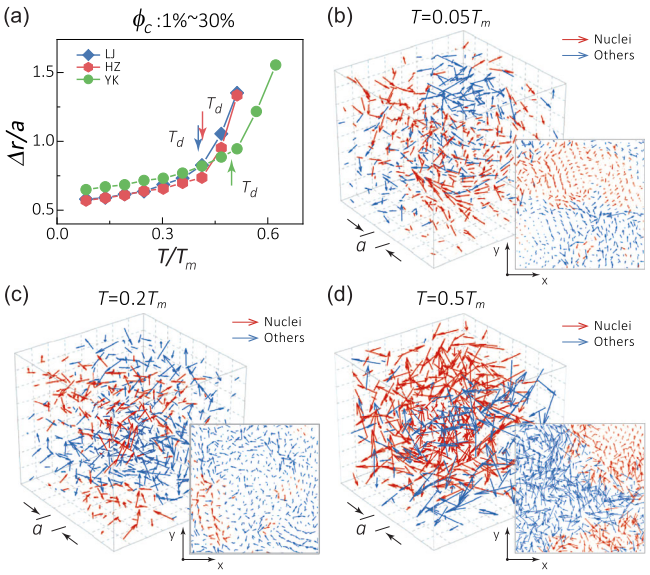

FIG. 2. Characterization of the particles' crystallization trajectory at low temperatures. (a) Temperature evolution of the mean particle displacement, Δr, from $\phi_c \approx 1\%$ to 30% for the LJ, HZ, and YK systems. The arrows point to T_d. (b)–(d) Particle displacement field in three dimensions and an x-y cross section of a part of the LJ system at three different temperatures. The length and direction of the arrows show the magnitude and direction of the particle displacements. Red color represents crystalline particles that form the nuclei at $\phi_c \approx 30\%$.

average interparticle distance a and only gradually grows with the increase of T. Going beyond T_d, Δr exhibits a much faster growth with temperature and quickly exceeds a. Accordingly, T_d should be a crossover temperature from a small-displacement subdiffusive crystallization mode to a diffusive mode, as illustrated by the three distinct displacement fields of crystallization in Figs. 2(b)–2(d).

Dynamical behaviors usually stem from some structural origins. Previous studies have suggested that the tetrahedra aggregations (TEAGs) are locally favored upon vitrification, and they serve as the prime geometric frustration against crystallization [6,7,16,17,48–50]. On the other hand, the precursor structures with good local bond orientational order but poor translational order facilitate nucleation in a diffusionless way [11,12,21,51]. Based on these understandings, we focus on the T-dependent evolution of TEAG and precursor particles, respectively. Particle i is a TEAG particle when it belongs to at least 12 adjacent quasiregular tetrahedra together with $q_6(i) < 0.27$ and $N_b(i) \geq 12$, where $N_b(i)$ is the number of nearest neighbors of particle i [7]. Precursor particles are defined as $0.27 < q_6 < 0.4$. The details are described in the SM [29]. Usually, a TEAG particle is the center of a defected icosahedron, whereas a precursor particle has a local crystalline bond orientational order.

We use the fraction of TEAG particles, ϕ_{TEAG}, and precursor particles, ϕ_{pre}, to probe the structure profile at the initial nucleation state ($\phi_c \approx 1\%$). When $T_g < T < T_d$, we find a sharp increase of ϕ_{TEAG} and the saturation of ϕ_{pre} towards supercooling, as shown in Figs. 3(a) and 3(b), respectively. It indicates that the low-temperature nucleation suffers high degrees of disorder besides the slow particle motion. However, a large number of precursor particles formed initially after the fast and deep quenching guarantee the successful generation of small crystal nuclei by slowly eradicating the quenched-in disorder inside precursors. Thus, the fastest nucleation should happen at T_d, where $\phi_{\mathrm{pre}}/\phi_{\mathrm{TEAG}}$ shows the maximum, as shown in Fig. 3(c).

With the increase of ϕ_{TEAG} towards T_p, we find that the TEAG particles percolate, as illustrated by the T dependence of the maximum spanning length l_m of the largest TEAG clusters in the system in Fig. 3(d). For the largest cluster, we calculate its lengths spanning over the three dimensions, l_x, l_y, and l_z, and define $l_m = \langle \max(l_x, l_y, l_z) \rangle$, with $\langle \cdots \rangle$ denoting the average over simulation runs. In regime I below T_p, the sum of ϕ_{TEAG} and ϕ_{pre} exceeds 40%, but we can still find the extremely slow crystallization through the precursor-to-solid conversion until the average amplitude of vibrational motion, e.g., $\Delta r^2 \sim 0.01a^2$ at T_g in Fig. S3 of the SM [29], is much smaller than the minimum particle displacement required for the diffusionless crystallization, e.g., $\Delta r \sim 0.6a$ in Fig. 2(a). We may further expect the onset of the mechanical stability of the system after the precursor-to-solid conversion is "frozen" when

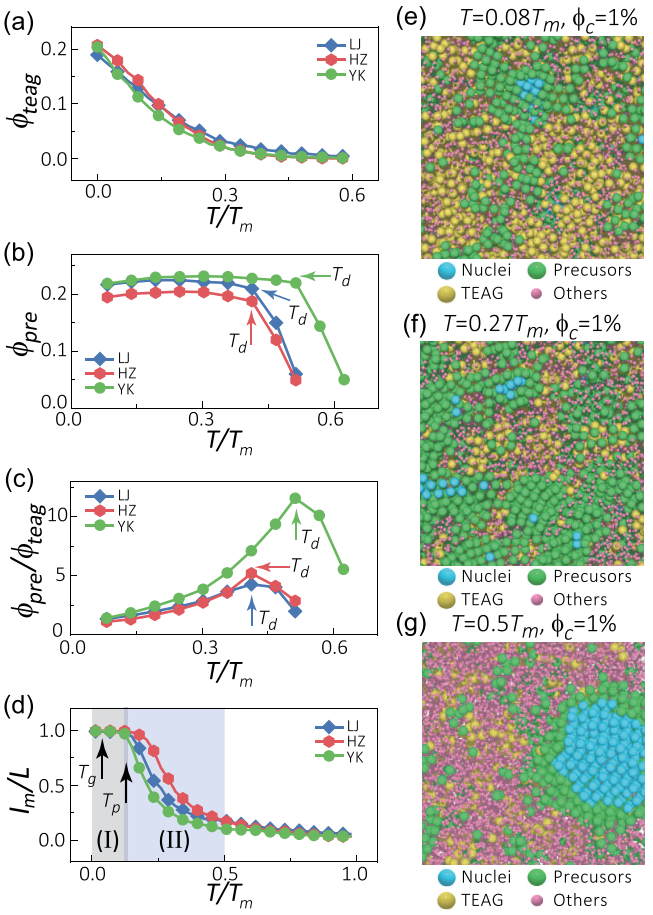

FIG. 3. T-dependent local-structure competition towards crystallization at low temperatures. (a)–(d) Temperature evolution of the fraction of TEAG particle ϕ_{TEAG}, precursor particles ϕ_{pre}, the ratio $\phi_{\mathrm{pre}}/\phi_{\mathrm{TEAG}}$, and the size of the maximum TEAG particle cluster l_m for the three systems. We calculate all these quantities at $\phi_c \approx 1\%$. (e)–(g) Spatial distribution of TEAG, precursor and crystalline particles at the initial nucleation stage at three representative temperatures (LJ system): $T_g < T < T_p$ in (e), $T_p < T < T_d$ in (f), and $T > T_d$ in (g). A thin slice of the three-dimensional system is shown. Note the distinct nuclei morphology for the three temperatures.

$T < T_g$. Accordingly, we do find the ceasing of crystallization when $T < T_g$ within the accessible simulation timescale, as shown in Fig. S3 of the SM [29].

The distinct nucleation behaviors in three temperature regimes can also be seen from the spatial distributions of TEAGs, precursor and crystalline particles, as shown in Figs. 3(e)–3(g).

In summary, by systematically studying the low-temperature nucleation kinetics, we reveal the particularity and significance of two characteristic temperatures, the maximum nucleation rate temperature T_d, and the glass transition temperature T_g. They divide the low-temperature regime into multiple parts with distinct crystallization scenarios. The particularly interesting part is

$T_g < T < T_d$, where we find the subdiffusive slow particle motion, the high degrees of geometric frustration, and the saturation of nucleation precursors. These multiple features indicate that the fastest nucleation is a delicate balance of TEAG and preordered precursors [22,23,25]. In this case, low-temperature nucleation proceeds through the diffusionless-like ordering of precursors, which appear as small-magnitude subdiffusive particle motions.

When $T < T_g$, we find the percolation of TEAG particles and low-amplitude vibrational motion to be much smaller than the particle displacement required for crystallization. We thus expect the system to have mechanical stability against the further ordering of precursors. In that case, diffusionless nucleation is obstructed. We also expect that the slow internal relaxations close to T_g actually affect the nucleation, as illustrated by the percolation of TEAG particles and drastic slow down of nucleation. In this crossover regime ($T_g < T < T_p$), the vibrational motion is not low enough, so that the sluggish crystal growth can still proceed through the slow internal relaxations, e.g., slow β or early-α glassy relaxation [4,5]. To facilitate the crystallization around or below T_g, some special approaches should be employed, e.g., introducing thermal annealing cycles or flat walls [46,52–55]. It is straightforward to expect that the characteristic temperatures concerned in this Letter may also play special roles in these approaches, which calls for follow-up studies.

We acknowledge financial support from the National Natural Science Foundation of China (No. 11734014, No. 12074355, No. 12174071, No. 12105050, and No. 12035004), the Innovation Program of Shanghai Municipal Education Commission (No. 2023ZKZD06), and the Science and Technology Commission of Shanghai Municipality (No. 22TQ003). We also thank the Supercomputing Center of University of Science and Technology of China for the computer time.

*ningxu@ustc.edu.cn
†tanpeng@fudan.edu.cn

[1] K. F. Kelton, *Crystal Nucleation in Liquids and Glasses* (Academic Press, Boston, 1991).
[2] P. G. Debenedetti, *Metastable Liquids: Concepts and Principles* (Princeton University Press, Princeton, NJ, 1996).
[3] A. Onuki, *Phase Transition Dynamics* (Cambridge University Press, Cambridge, England, 2002).
[4] P. G. Debenedetti and F. H. Stillinger, Nature (London) **410**, 259 (2001).
[5] L. Berthier and G. Biroli, Rev. Mod. Phys. **83**, 587 (2011).
[6] C. P. Royall and S. R. Williams, Phys. Rep. **560**, 1 (2015).
[7] H. Tanaka, H. Tong, R. Shi, and J. Russo, Nat. Rev. Phys. **1**, 333 (2019).
[8] P. Rein ten Wolde and D. Frenkel, Science **277**, 1975 (1997).
[9] S. Auer and D. Frenkel, Nature (London) **409**, 1020 (2001).
[10] F. Trudu, D. Donadio, and M. Parrinello, Phys. Rev. Lett. **97**, 105701 (2006).
[11] T. Kawasaki and H. Tanaka, Proc. Natl. Acad. Sci. U.S.A. **107**, 14036 (2010).
[12] J. Russo and H. Tanaka, Sci. Rep. **2**, 505 (2012).
[13] J. Wedekind, L. Xu, S. V. Buldyrev, H. E. Stanley, D. Reguera, and G. Franzese, Sci. Rep. **5**, 1 (2015).
[14] J. F. Lutsko, Sci. Adv. **5**, eaav7399 (2019).
[15] R. P. Sear, J. Chem. Phys. **128**, 214513 (2008).
[16] F. C. Frank, Proc. R. Soc. A **215**, 43 (1952).
[17] C. Xia, J. Li, Y. Cao, B. Kou, X. Xiao, K. Fezzaa, T. Xiao, and Y. Wang, Nat. Commun. **6**, 8409 (2015).
[18] N. Francois, M. Saadatfar, R. Cruikshank, and A. Sheppard, Phys. Rev. Lett. **111**, 148001 (2013).
[19] M. Leocmach and H. Tanaka, Nat. Commun. **3**, 974 (2012).
[20] G. Sun, J. Xu, and P. Harrowell, Nat. Mater. **17**, 881 (2018).
[21] P. Tan, N. Xu, and L. Xu, Nat. Phys. **10**, 73 (2014).
[22] G. I. Tóth, T. Pusztai, G. Tegze, G. Tóth, and L. Gránásy, Phys. Rev. Lett. **107**, 175702 (2011).
[23] H. Emmerich, H. Löwen, R. Wittkowski, T. Gruhn, G. I. Tóth, G. Tegze, and L. Gránásy, Adv. Phys. **61**, 665 (2012).
[24] S. Tang, J. C. Wang, and B. Svendsen, and D. Raabe, Acta Mater. **139**, 196 (2017).
[25] L. Gránásy, G. I. Tóth, J. A. Warren, F. Podmaniczky, G. Tegze, L. Rátkai, and T. Pusztai, Prog. Mater. Sci. **106**, 100569 (2019).
[26] M. Li, Y. S. Chen, H. Tanaka, and P. Tan, Sci. Adv. **6**, eaaw8938 (2020).
[27] H. Tanaka, Eur. Phys. J. E **35**, 113 (2012).
[28] H. Shintani and H. Tanaka, Nat. Phys. **2**, 200 (2006).
[29] See Supplemental Material at http://link.aps.org/supplemental/10.1103/PhysRevLett.130.178201 for supportive information and results, which includes Refs. [21,26,30–36].
[30] P. J. Steinhardt, D. R. Nelson, and M. Ronchetti, Phys. Rev. B **28**, 784 (1983).
[31] J. Russo and H. Tanaka, Soft Matter **8**, 4206 (2012).
[32] T. C. Hales, Ann. Math. **162**, 1065 (2005).
[33] N. N. Medvedev and Y. I. Naberukhin, J. Non-Cryst. Solids **94**, 402 (1987).
[34] I. L. Dryden and K. V. Mardia, *Statistical Shape Analysis* (John Wiley & Sons, New York, 1998).
[35] A. V. Anikeenko and N. N. Medvedev, Phys. Rev. Lett. **98**, 235504 (2007).
[36] F. C. Frank and J. S. Kasper, Acta Crystallogr. **11**, 184 (1958).
[37] J. P. K. Doye and D. J. Wales, Phys. Rev. Lett. **86**, 5719 (2001).
[38] H. Tanaka, T. Kawasaki, H. Shintani, and K. Watanabe, Nat. Mater. **9**, 324 (2010).
[39] S. Karmakar, C. Dasgupta, and S. Sastry, Annu. Rev. Condens. Matter Phys. **5**, 255 (2014).
[40] P. Rein ten Wolde, M. J. Ruiz-Montero, and D. Frenkel, J. Chem. Phys. **104**, 9932 (1996).
[41] P. Rein ten Wolde and D. Frenkel, Phys. Chem. Chem. Phys. **1**, 2191 (1999).
[42] D. Moroni, P. Rein ten Wolde, and P. G. Bolhuis, Phys. Rev. Lett. **94**, 235703 (2005).

[43] W. Lechner and C. Dellago, J. Chem. Phys. **129**, 114707 (2008).
[44] W. Mickel, S. C. Kapfer, G. E. Schröder-Turk, and K. Mecke, J. Chem. Phys. **138**, 044501 (2013).
[45] S. Arai and H. Tanaka, Nat. Phys. **13**, 503 (2017).
[46] Q. Gao, J. Ai, S. Tang, M. Li, Y. Chen, J. Huang, H. Tong, L. Xu, L. Xu, H. Tanaka, and P. Tan, Nat. Mater. **20**, 1431 (2021).
[47] C. Sinn, A. Heymann, A. Stipp, and T. Palberg, Prog. Colloid Polym. Sci. **118**, 266 (2001).
[48] J. F. Sadoc, AIP Conf. Proc. **489**, 105 (1999).
[49] G. Tarjus, S. A. Kivelson, Z. Nussinov, and P. Viot, J. Phys. Condens. Matter **17**, R1143 (2005).
[50] S. Marín-Aguilar, H. H. Wensink, G. Foffi, and F. Smallenburg, Phys. Rev. Lett. **124**, 208005 (2020).
[51] T. Schilling, H. J. Schöpe, M. Oettel, G. Opletal, and I. Snook, Phys. Rev. Lett. **105**, 025701 (2010).
[52] A. Cacciuto, S. Auer, and D. Frenkel, Nature (London) **428**, 404 (2004).
[53] G. I. Tóth, G. Tegze, T. Pusztai, and L. Gránásy, Phys. Rev. Lett. **108**, 025502 (2012).
[54] G. Liu and S. J. Fonash, Appl. Phys. Lett. **55**, 660 (1989).
[55] J. Liu, C. Gao, X. He, Q. Ye, L. Ouyang, D. Zhuang, C. Liao, J. Mei, and W. Lau, ACS Appl. Mater. Interfaces **7**, 24008 (2015).